PLANETARY CRATER DETECTION AND REGISTRATION USING MARKED POINT PROCESSES, GRAPH CUT ALGORITHMS, AND WAVELET TRANSFORMS

Alberto Gotelli², Jacqueline Le Moigne¹, Gabriele Moser², Sebastiano B. Serpico²

¹ NASA Goddard Space Flight Center, Greenbelt, MD 20771, jacqueline.j.lemoigne-stewart@nasa.gov
² University of Genoa, DITEN Dept., Via Opera Pia 11a, 16145 Genoa, Italy, gabriele.moser@unige.it

ABSTRACT

This paper addresses the problem of semi-automatic image registration on planetary images. A joint feature-based and area-based approach is proposed. Firstly, the most relevant craters are extracted from the two images to register, and then, registration is performed in two steps. The first step matches the craters extracted from the images based on a generalized Hausdorff distance. In the second step, the mutual information between the two images is maximized to achieve high registration accuracy. Craters are detected by a stochastic-geometry approach based on a marked point process model and of a multiple-birth-and-cut energy minimization algorithm. The experimental validation is carried out with 13 images for the crater extraction stage, and with 20 semi-synthetic pairs of images with ground truth and several images extracted from actual multi-temporal lunar scenes for the registration phase.

Index Terms — Marked Point Processes, Multiple Birth and Cut, Featured-Based Image Registration, Area-Based Image Registration, Mutual Information, Planetary Images.

1. INTRODUCTION

An increasing number of images have been collected by different planetary missions over the past few decades. The collected data exhibit different characteristics that depend on the kind of sensor employed, the time of acquisition, the illumination conditions, etc. To benefit from the wealth of information provided by these multiple data sets, (semi) autonomous and fast registration is necessary, since it allows the comparison and fusion of data acquired by different sensors and/or at different times. In the literature the problem of image registration is generally approached in one of the following three ways: 1. based on ground control points or other spatial features, such as from a scale-invariant feature transform (SIFT) [1]; 2. considering the entire image area and making comparisons based on some global area-wise metric, such as the mutual information [2]; 3. through Fourier, wavelet, or shearlet transforms [3], [4]. The goal of this work is to achieve high accuracy and (semi) autonomous registration of planetary images. A joint feature-based / area-based approach is used. A good feature extraction procedure is the first step to achieve the objective, since registration generally requires prior accurate extraction of spatial features. Different types of spatial structures of variable size and shape characterize planetary surfaces. Among the typical features, craters play a primary role. In order to overcome the typical problems of planetary images with limited contrast, poor illumination, and a lack of good features, an unsupervised approach for the extraction of planetary craters, based on a marked point process (MPP) is employed in this work, extending the previous work in [5]. The framework is stochastic and the goal is to minimize an energy function on the state space of all possible configurations of objects (craters), using a multiple birth and cut (MBC) algorithm.

After this feature extraction step, the actual registration technique proceeds as follows: first, a generalized pattern search algorithm minimizes an energy function that matches the features extracted from the two images to register; then, the maximization of the area-based mutual information (MI) between the two images is performed in a smaller search space using simulated annealing. This two-step process aims at jointly combining the well-known accuracy of MI-based registration, sensitivity to the main spatial features in the input data, and computational efficiency.

2. METHODOLOGY

The proposed method is structured as follows: (i) first, crater extraction is performed as a first step to extract useful features for registration; (ii) then, the minimization of a function that describes the relationship between the features extracted from the reference and input images is performed; (iii) finally, the maximization of the mutual information between the two images in a small neighborhood of the transformation found at step (ii) allows highly precise registration to be achieved.

2.1 Crater Detection

Following the high detection rate of different objects reported in [7], and considering the previous works with the same goals in [5] and [6], an MPP-based approach, aimed at detecting elliptical objects, is proposed here for crater detection.

2.1.1. Marked Point Processes

The MPP framework defines probabilistic models on configuration spaces consisting of an unknown number of parametric objects. Markov properties allow the introduction of local interactions and the definition of a prior on the object distribution in the scene. This framework can be interpreted

as a generalization of the Markov random field (MRF) theory, where the number of random variables is unknown and are not associated with a predefined pixel lattice. Moreover, an object is associated with each variable, on which some geometric constraints can be modeled.

Given a bounded subset P of $\Re^2$, a point process X is a measurable mapping from a probability space (Ω, A, p) (where Ω is the certain event, A is the event space, and p is a probability measure) to configurations of points on P, i.e., a random variable whose realizations are random configurations x of points:

$$x = \{x_1, \dots, x_n\},$$

where $x_i \in P$ is the i-th point in the image plane. These configurations belong to a measure space (Ψ, B, μ) where Ψ is the collection of all finite subsets of P, B is a σ-algebra over Ψ, and μ is a measure on the configuration space. An MPP is a point process defined by a density function with respect to the Poisson measure.

A configuration of an MPP consists of a set of marked points, i.e. a set of parameters associated with each point. In image analysis, these parameters are geometrical features related to that particular point. So, it is possible to state that each realization of an MPP represents a model for the spatial distribution of several objects in the scene. The probability distribution of an MPP is uniformly continuous with respect to a Poisson measure on S.

2.1.2. MPP Formalization for Crater Extraction
A crater can be modeled as an ellipse with low eccentricity. In this sense, it is possible to define an MPP where the objects are ellipses, so each point has the characteristics features of an ellipse as marks. In this work five parameters have been adopted to characterize the ellipse: the center coordinates (b, c), the major axis a, the eccentricity e, and the orientation angle ϑ. (b, c) is a Poisson point in the image plane, while (a, e, ϑ) is the corresponding mark; n such 5-tuples are a realization of the MPP X used here for crater detection.

In particular, a binary image I_g that shows the object boundaries in the image is first computed through Canny's filter. Then, I_g is modeled as a configuration of ellipses whose positions and attributes are realizations of the MPP X.

2.1.3. The Proposed Energy Function
Similar to the case of MRFs, Bayesian inference with MPPs can be formalized in terms of minimum-energy problems. The energy function must take into account both the possible interactions between the geometric objects $x_1, x_2, \dots, x_n$ in the configuration x and the way they fit the data (in particular, the extracted contours).

So, starting from [5], the energy is divided into two terms, a prior contribution and a likelihood component:

$$U(x|I_g) = U_p(x) + U_L(I_g|x).$$

The prior U_p describes the general aspect of the desired solution. In our case, it is useful to penalize overlapping

craters, so U_p is defined so that it grows with the overlapping area between two ellipses and saturates when they overlap more than 10% of their overall area:

$$U_p(x) = \begin{cases} \dfrac{1}{n} \displaystyle\sum_{x_i * x_j} \dfrac{x_i \cap x_j}{x_i \cup x_j} & if \ x_i \cap x_j \leq 0.1 \ x_i \cup x_j \\ 1 & otherwise \end{cases}$$

where $x_i \cap x_j$ and $x_i \cup x_j$ denote the areas of the intersection and the union of the ellipses x_i and x_j in the configuration x and $x_i * x_j = $ true if and only if the intersection is nonempty. Then, the likelihood term U_L is defined as:

$$U_L(I_g|x) = U_D(I_g|x) + U_S(I_g|x),$$

where U_D represents a measure of distance between the configuration and the contours extracted from the data, and U_S is a measure of similarity between the configuration and the data. U_S is defined as a correlation measure:

$$U_S(I_g|x) = -\frac{\left|\{(u,v): I_g(u,v) = 1 \ \& \ \prod(u,v|x) = 1\}\right|}{\left|\{(u,v): N_g(u,v|x) = 1\}\right|},$$

where (u, v) are the spatial coordinates in the image plane; $\prod(u, v|x)$ is the projection of the configuration x such that $\prod(u, v|x) = 1$ if (u, v) belongs to the boundary of at least one ellipse in x; $N_g(u, v|x)$ is an annulus around each ellipse and is used to consider just the neighborhood pixels and not to penalize small ellipses; and there is a minus sign so that minimizing energy favor maximizing correlation.

The data term U_D, is computed at the object level: for each ellipse in the configuration, the distance from the extracted Canny contour points is computed:

$$U_D(I_g|x) = \sum_i \frac{d(x_i, \{(u,v): I_g(u,v) = 1\})}{a_i}$$

where the major axis a_i of each ellipse is included for normalization purposes. The distance d adopted in this work is the Hausdorff distance.

2.1.4. Multiple Birth and Cut (MBC)
Common (e.g., direct or gradient-based) minimizers are often not effective for the minimization of the energy of an MPP because the minimization problem is challenging with many local minima and a huge search space. On the contrary, MBC was shown to be an efficient tool for the minimization of MPP energies [7]. It is based on graph cuts and is iterative:

Initialization of the number R of ellipses to be added in each iteration and of the iteration count $t = 0$, and generation of an initial configuration of ellipses ω_0. R only impacts convergence speed and not detection accuracy.

Birth Step: Generation of a new configuration ω' of R non-overlapping ellipses in the scene by sampling R new ellipses according to a posterior probability distribution proportional to $\exp[-U(x|I_g)]$ [7].

Graph Construction: a graph is constructed for $\omega = \omega_t \cup \omega'$. Each node represents an ellipse. Edges link ellipses to each other and to terminal nodes (source and sink) to be used for the Max-Flow/Min-Cut processing of graph cut

optimization. Edge weights are assigned to both types of link according to energy terms: details can be found in [7].

Graph Cut: the Max-Flow/Min-Cut algorithm in [8] is applied to perform a binary classification between surviving and removed ellipses (see [7] for details).

Convergence: the steps listed above are iteratively repeated until the cut returns the same configuration for a predefined (large) number of consecutive times.

2.1.5. Wavelet Decomposition

Since the computational burden of MBC strongly depends on the size of the input image, wavelet decomposition is used to obtain an important speed-up factor. A decimated 2D discrete wavelet transform is applied to the input image. In particular, four levels of decomposition are computed by keeping at each step only the low-pass transformed image. Then, the crater detection algorithm is applied recursively from the coarsest-level decomposed image going back until the original image. At each step, all the regions where ellipses have been found at the previous (coarser) levels are removed from the search space, by erasing the corresponding Canny contours. Therefore, a substantial reduction in computation time is obtained without sacrificing detection accuracy.

2.2. Image Registration

The registration is performed in two steps: the first one matches the extracted features from both images, while the second one maximizes the mutual information in a small neighborhood of the transformation obtained by the first step.

2.2.1. First Step of Registration

According to the nature of the two images to be registered it is possible to match the craters extracted from the reference image with the Canny contours extracted from the input image, or to match the craters extracted from both the reference and input images. In the former case, the minimization is performed on a functional $U_{tot}(p)$ which is similar to the likelihood term of the aforementioned energy and is a function on the vector p of the parameters of a Rotation Scale Translation (RST) transformation:

$$U_{tot}(p) = \sum_{i=1}^{n} \frac{d(x_i, I_g^p)}{a_i} - \frac{\left\{ (u,v) \in I_g^p : \Pi(u,v|x) = 1 \right\}}{|I_g^p|}$$

where I_g^p is the RST transform of the set $\left\{ (u,v) : I_g(u,v) = 1 \right\}$ of Canny contour points. In the latter case, the minimization is performed by minimizing the Hausdorff distance between the ellipses extracted in the two images. This second option is especially useful in the case of multi-temporal images in which Canny contours differ substantially at distinct observation times. In both cases, minimization is performed by considering user-defined rectangular crops of the images to be registered, in which at least two craters are present. On one hand, this human-in-the-loop component makes the procedure not fully automated. On the other hand, the proposed method largely reduces the need for human intervention as compared to classical interactive registration procedures based on the selection of control points. Furthermore, this region-of-interest selection can be automated as well.

The minimization of $U_{tot}(p)$ is performed using a generalized pattern search (GPS) algorithm [10] where the mesh is created with the GPS Positive basis 2N method and the search phase is performed through a genetic algorithm.

2.2.2. Second Step of Registration

The first step gives a transformation result p'. To improve registration performances, a further step of maximization of the mutual information between the two images is also performed in a neighborhood of p', thus finding a further RST transformation p''. The maximization is performed using simulated annealing.

3. EXPERIMENTAL RESULTS

Three sets of experiments have been conducted. The first set deals with the accuracy of crater detection. The second set deals with the evaluation of registration performances on semi-synthetic data for which the reference image is a real planetary image and the input image is an RST transform of the reference image (with some additive Gaussian noise). For these experiments, the ground truth transformation is always available and performances can be evaluated quantitatively through the root mean square (RMS) error between the computed and the true transformations [9]. The third set of experiments deals with the registration of pairs of multi-temporal images; in this case the data are fully real, so the evaluation of the performances is performed using a checkered visual representation where squares are taken successively from the reference and the input image.

3.1. Crater Detection Results

Crater detection accuracy has been tested on 12 different images taken by the Thermal Emission Imaging System (THEMIS) or High Resolution Stereo Camera (HRSC) sensors orbiting around Mars. The results present a high precision of detection, but not all the craters have been found: this is due to the fact that for registration purposes the focus was in the bigger craters. Table 1 presents the quantitative results for crater detection. The three quantities in the table are defined as follow:

$$D = 100 \cdot \frac{TP}{TP+FN} \quad B = \frac{FP}{TP} \quad Q = 100 \cdot \frac{TP}{TP+FP+FN}$$

where TP are the true positives, FN the false negatives and FP the false positives.

Table 1 - Quantitative results for crater detection

Data	D (%)	B	Q (%)
THEMIS	81.5	0	81.5
HRSC	73.7	0	73.7
Average	77.6	0	77.6

Please note that B is always equal to zero because in all the experiments no false positives were present. The reason lies in the way the algorithm was designed: since the extraction of the craters from the image scene is important for

registration purposes, it is better to find fewer craters without any false alarm rather than finding craters that do not exist.

4.2. Registration Results: Semi-Synthetic Data

The simple minimization of an energy function that matches the extracted craters of the reference image with the contours of the input image gives good results. Then, the introduction of a final step of maximization of the mutual information allows to significantly decrease the RMS found after the first step of registration, guaranteeing the registration RMS to be always under the unity. Table 2 reports the average values of the RMS found by applying the algorithm to 20 different couples of semi-synthetic data, each obtained from 10 THEMIS and 10 HRSC images. Subpixel accuracy was obtained in all cases. These results suggest the effectiveness of the proposed method.

Table 2 - RMS results on two different sensors.

Image Pairs	Average RMS
On 10 THEMIS images	*0.54*
On 10 HRSC images	*0.59*
On all 20 images	*0.565*

4.3. Registration Results: Real Data

Figure 1 shows an example of registration results obtained from a couple of multi-temporal images of the Moon surface acquired by the Lunar Reconnaissance Orbiter Camera (LROC).
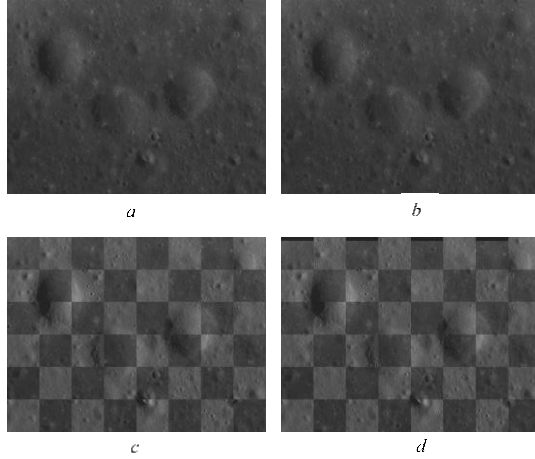

Figure 1 - (a) reference image, (b) input image, (c) and (d) checkered representation before and after registration transformation vector for registration found:
$[t_x = 13.01;\ t_y = -28.78;\ scale = 1;\ \vartheta = 0.01]$

For these experiments the ground-truth transformation is not available so, a representation as the one in the figure above, is a good way to understand the goodness of the registration procedure. Several tests have been conducted on images similar to the ones in Figure 1, achieving always good registration accuracy.

5. CONCLUSION

In this work, the problem of registering planetary images acquired has been addressed. Experiments with data from three sensors orbiting around Mars and the Moon has suggested that the proposed approach, based on crater extraction through MPPs and a two-step registration process, is effective. High accuracy was also obtained in the crater detection phase by itself. These results suggest that the proposed formalization of this detection problem through an MPP model in a stochastic geometry framework is effective. Indeed, the flexibility of MPP modeling in characterizing random distributions of parameterized objects in the image plane, which was proven in several applications to road, building, tree, flamingo, boat, etc., detection, was confirmed in this application to crater extraction from planetary data as well. In future work, the method will be further tested for the registration of multi-sensor images.

6. REFERENCES

[1] D. G. Lowe, "Object recognition from local scale-invariant features," *7th IEEE International Conference of Computer Vision,* vol. 2, pp. 1150-1157, 1999.

[2] P. Thévenaz and M. Unser, "Optimization of mutual information for multiresolution image registration," *IEEE Transaction of Image Processing,* vol. 9, no. 12, pp. 2089-2099, 2000.

[3] H. Shakir, S. T. Ahsan and N. Faisal, "Multimodal medical image registration using discrete wavelet transform and Gaussian pyramids," in *2015 IEEE International Conference on Imaging Systems and Techniques (IST)*, Macau, 2015.

[4] J. M. Murphy, J. Le Moigne and D. J. Harding, "Automatic Image Registration of Multimodal Remotely Sensed Data With Global Shearlet Features," *IEEE Transactions on Geoscience and Remote Sensing,* vol. 54, no. 3, pp. 1685-1704, 2016.

[5] G. Troglio, J. A. Benediktsson, G. Moser and S. B. Serpico, "Crater Detection Based on Marked Point Processes," in *Signal and Image Processing for Remote Sensing*, Boca Raton, FL, CRC Press, 2012, pp. 325-338.

[6] G. Troglio, J. Le Moigne, J.A. Benediktsson, G. Moser, and S.B. Serpico, "Automatic Feature Extraction from Planetary Images," *IEEE Geoscience and Remote Sensing Letters*, **Vol. 9**, No. 1, pp. 95-99, January 2012.

[7] E. Soubies, P. Weiss and X. Descombes, "Graph Cut Based Segmentation of Predefined Shapes: Applications to Biological Imaging," *Pattern Recognition Applications and Methods, Advances in Intelligent Systems and Computing,* p. 318, 2015.

[8] Y. Boykov, O. Veksler and R. Zabih, "Fast Approximate Energy Minimization via Graph Cuts," *IEEE Transactions on Pattern Analysis and Machine Intelligence,* vol. 23, no. 11, pp. 1222-1239, 2001.

[9] I. Zavorin and J. Le Moigne, "Use of Multiresolution Wavelet Feature Pyramids for Automatic Registration of Multisensor Imagery," *IEEE Transactions on Image Processing*, vol. 14, no. 6, 2005.

[10] C. Audet and J. E. J. Dennis, "Analysis of Generalized Pattern Searches," *SIAM Journal on Optimization,* vol. 13, no. 3, pp. 889-903, 2003.